

Crystallization of Ca^+ ions in a linear rf octupole ion trap

Kunihiko Okada,* Kazuhiro Yasuda, and Toshinobu Takayanagi
Department of Physics, Sophia University, 7-1 Kioicho, Chiyoda, Tokyo 102-8554, Japan

Michiharu Wada
Atomic Physics Laboratory, RIKEN, 2-1 Hirosawa, Wako, Saitama 351-0198, Japan

Hans A. Schuessler
Department of Physics, Texas A&M University, College Station, Texas 77843, USA

Shunsuke Ohtani
Institute for Laser Science (ILS), University of Electro-Communications, 1-5-1 Chofugaoka, Chofu, Tokyo, 182-8585, Japan
 (Received 15 November 2006; published 22 March 2007)

A laser-cooling experiment with Ca^+ ions trapped in a linear rf octupole ion trap is presented. The phase transition of the laser-cooled Ca^+ ions from the cloud to the crystal state is observed by an abrupt dip of the laser-induced fluorescence spectrum and indicates that mK temperatures are obtained. We have also performed molecular dynamics simulations under various conditions to confirm this property by deducing axially symmetric structures of Coulomb crystals and by evaluating the translational temperatures of the laser-cooled ions. The simulation results show that for small numbers of ions novel ring-shaped crystals are produced. As the number of ions is increased, cylindrical layers in the ring crystal are sequentially formed. For more than 100 ions, also hexagonal and spiral structures emerge in parts of the large-size ion crystal, which has a length on the order of millimeters for the present geometrical arrangement and voltages. An advantage of the linear rf octupole trap is its large almost-field-free region in the middle of the trap, where the micromotion amplitude is small for trapped ions. These results demonstrate that such a multipole trap has attractive features for quantum computing and ultracold ion-atom collision studies.

DOI: [10.1103/PhysRevA.75.033409](https://doi.org/10.1103/PhysRevA.75.033409)

PACS number(s): 32.80.Pj, 39.90.+d, 42.50.Vk, 52.27.Jt

I. INTRODUCTION

Coulomb crystals of laser-cooled alkaline-earth-metal and other ions are an interesting research object because there are many applications—e.g., a microwave standard based on ion crystals, quantum computing [1–3], tools for studying non-neutral plasma physics [4–6], the formation of cold molecular ions by sympathetic cooling [7–9], and tests of a possible variation of the fundamental physical constants and physical principles [10–12]. To our knowledge, laser-cooling experiments in a linear rf multipole ion trap and in particular an octupole trap have so far not been performed, although Coulomb crystals in other ion traps were studied in detail at many institutes [8,13–20].

In the case of the linear quadrupole Paul trap, a small number of ions initially align themselves along the central trap axis like a string. As the number of ions increases, the shape of the Coulomb crystal gradually changes to cylindrical layers of prolate (oblate) shape [5]. In contrast to these well-studied structures, new features of Coulomb crystals not present in a linear quadrupole trap arise in a multipole trap due to the large almost-field-free region in the middle of this trap [21]. In principle, a large number of cold ions can be trapped, since the trapping volume of the multipole trap is larger than that of the linear Paul trap of comparable size. This feature is of particular advantage for highly stable ion

clocks to support space-borne applications [22].

It is well known that the adiabatic radial pseudopotential [21] for a single trapped ion in a linear rf octupole ion trap is given by

$$\phi_{\text{psd}}(r) = \frac{4q^2 V_{\text{ac}}^2}{mr_0^8 \Omega^2} r^6, \quad r = \sqrt{x^2 + y^2}, \quad (1)$$

where q is the charge of the trapped ion, V_{ac} is the amplitude of the radio frequency (rf) voltage applied to adjacent rod electrodes, m is the mass of the ion, and $\Omega/2\pi$ is the operating frequency of the ion trap. For axial confinement of ions, the electrodes are normally segmented into three or more parts and the static voltage V_{z0} is applied to the outside sets of segmented electrodes. The static potential is given by

$$\phi_s(x, y, z) = \frac{\kappa V_{z0}}{z_0^2} \left(z^2 - \frac{x^2 + y^2}{2} \right), \quad (2)$$

where $2z_0$ is the length of the center part of the segmented trap. The geometrical factor κ is determined by the particular geometry of the octupole trap. The flatness of the radial pseudopotential of Eq. (1) provides novel features for crystallized ions, since the static potential ϕ_s gives a small distortion to ϕ_{psd} (see Fig. 3). As a consequence, it is expected that laser-cooled ions are distributed like a ring and the structures of these ring Coulomb crystals are changed by variations of V_{z0} . For very large ion numbers also the inner regions of the octupole trap are expected to be filled up as cylindrical rings of smaller diameters develop, similar to

*Electronic address: okada-k@sophia.ac.jp

what was observed with increasing ring diameters in a linear quadrupole ion trap [5].

One of our experimental plans is to produce planar Coulomb crystals using a suitably chosen multipole trap. As a first step towards that goal, we chose a linear rf octupole ion trap for testing the performance of rf multipole traps in laser-cooling experiments. As described in the following sections, we numerically simulate the case where ring-shaped Coulomb crystals are produced by laser-cooled ions in a linear rf octupole trap. Such a two-dimensional structure of a Coulomb crystal is novel and could be useful for quantum computing using laser-cooled ions.

The other experimental plan is to measure the reaction rates of astrophysically important chemical reactions, such as $\text{NH}_3^+ + \text{H}_2(\text{D}_2)$ [23–25], at an ultracold temperature using the sympathetic cooling method [7,8,26–29]. The experimental realization of sympathetic crystallization of molecular ions in the octupole trap is challenging. As an initial step, we have studied sympathetic cooling of molecular ions by molecular dynamics (MD) simulations to explore the possibility to produce cold molecular ions in the linear rf octupole trap. In this simulation study, we found that the sympathetically crystallized light molecular ions by laser-cooled heavy ions migrate to the inner part of the linear octupole trap, where the micro-motion amplitude is smaller and the sympathetic cooling is effective for the molecular ions. These studies are reported elsewhere [30].

In this paper, we describe laser-cooling experiments performed with a linear rf octupole trap. Both experimental measurements and MD simulations were carried out. The paper is arranged as follows. First, we present the results of a laser-cooling experiment with trapped Ca^+ ions in Sec. II. In it the phase transition of the laser-cooled Ca^+ ions was confirmed by the observation of an abrupt dip of the laser-induced fluorescence (LIF) spectrum. These fluorescence spectra show all the features (line shape, laser intensity, laser frequency, and ion number dependence) known from laser-cooling studies with linear quadrupole traps. In Secs. III and IV, MD simulations were carried out to deduce the particular shapes of the Coulomb crystals and to determine the translational temperatures of the Ca^+ ions. The results of a systematic study of the expected forms of Coulomb crystals as functions of the number of ions and the trapping parameters are also presented. A LIF spectrum with an abrupt dip is simulated to explain also the influence of rf heating on the octupole trap. In this section a particular, not planar form of a large size Coulomb crystal is selected and its interwoven cylindrical structure is described. Finally, a summary is given in Sec. V.

II. EXPERIMENT

A schematic diagram of the central part of the linear rf octupole ion trap is shown in Fig. 1. The octupole trap consists of eight cylindrical electrodes, which are sectioned into three sets. For confinement in the radial direction, rf voltages with inverted phases are alternately applied to adjacent rod electrodes. The inner radius of the trap is $r_0 = 7.5$ mm, and the diameter of the cylindrical electrodes is 5 mm. The

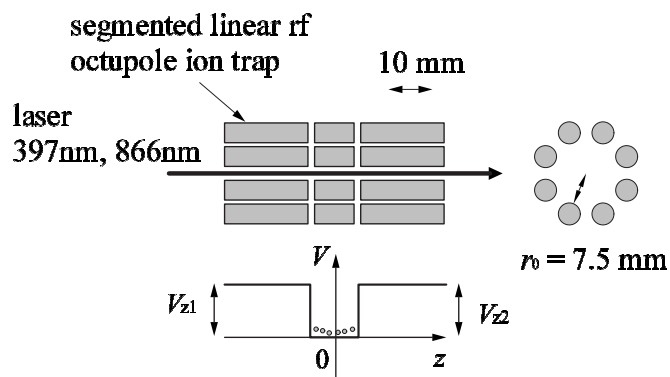


FIG. 1. Schematic diagram of the central part of the linear rf octupole trap. The lower part shows the arrangement of the static voltages of V_{z1} and V_{z2} applied to the set of side electrodes.

length of the center electrode of the segmented trap is $2z_0 = 10$ mm. The driving rf frequency and the amplitude are typically $f_{\text{rf}} = 10$ MHz and $V_{\text{ac}} = 370$ V, respectively. Static voltages (V_{z1} , V_{z2}) of up to about 300 mV are normally applied to the set of side electrodes to confine ions in the middle section along the axial direction. The linear rf octupole trap is mounted on a cryogenic vessel, which can be filled with liquid nitrogen or liquid helium [31,32]. In the present laser-cooling experiment, the trap electrodes are cooled to approximately 100 K by liquid nitrogen to avoid loss of trapped ions as much as possible. The ion trap is enclosed in a vacuum chamber evacuated to below 1×10^{-7} Pa. The laser ablation method is applied to produce Ca^+ ions from a Ca metal piece located outside the ion trap. Before the ion production process, we admit helium gas at about 10^{-4} Pa for efficient trapping and buffer gas cooling of Ca^+ ions. This process promotes also the accumulation of the ions to the middle of the trap so that the laser cooling can subsequently become effective. Then, we close the leak valve and quickly pump to ultrahigh vacuum when we apply the laser cooling.

For the laser cooling of trapped Ca^+ ions, we used two grating-stabilized diode lasers with oscillation wavelengths at 397 nm and 866 nm [33]. The wavelengths correspond to the two optical dipole transitions of the $4s^2 S_{1/2} \rightarrow 4p^2 P_{1/2}$ and the $3d^2 D_{3/2} \rightarrow 4p^2 P_{1/2}$, respectively. The cooling transition is at 397 nm. The laser light at 866 nm is necessary to prevent optical pumping into the metastable $^2D_{3/2}$ state. The lifetime of the $P_{1/2}$ state is 7.14 ns which corresponds to a natural linewidth of 22 MHz [34]. The available powers of the cooling laser and the repumper are 0.2 mW and 2 mW, respectively. Two commercial wavemeters (Burleigh, WA-1000 and Advantest, TQ8325) are used to monitor the absolute wavelengths of the lasers. The relative frequency of the 397 nm laser is monitored by a confocal Fabry-Perot (CFP) cavity with a length of 150 mm. The LIF at 397 nm is focused on a photomultiplier tube (Hamamatsu Photonics, R464) located at right angles to the trap axis. The photon-counting signal is recorded by a computer. An interference filter for 397 nm is used for the reduction of background photons. The geometrical detection efficiency of the optics is estimated by a Monte Carlo simulation to be 1.4%, and the

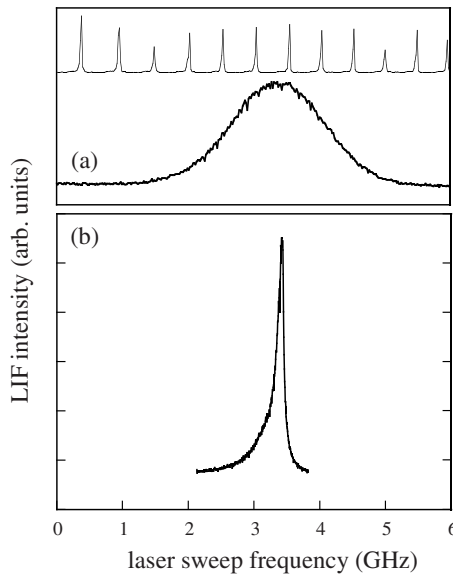


FIG. 2. (a) Laser-induced fluorescence spectrum of helium buffer-gas-cooled ions *without* liquid nitrogen cooling. The number of Ca⁺ ions in the cloud is estimated to be about 1.5×10^3 . Helium buffer gas is present, at room temperature and a pressure of 1.4×10^{-4} Pa. (b) Laser-induced fluorescence spectrum of a laser-cooled ion cloud obtained by scanning the laser frequency at 11 MHz/s over the resonance position under the ultrahigh-vacuum condition. The number of Ca⁺ ions in the cloud is about 1×10^3 . The HWHM of the spectrum is $\Delta\nu = 108(2)$ MHz, which corresponds to an ion temperature of 12.7(5) K. The upper trace shows the reference signal from the CFP cavity with a length of 150 mm. Experimental parameters of the ion trap are $f_{\text{rf}} = \Omega/2\pi = 9.978$ MHz, $V_{\text{ac}} = 370$ V, and $V_{z1} = V_{z2} = 83$ mV.

total detection efficiency including the losses of the optics is about 3×10^{-4} .

Figure 2 shows the LIF spectra of both buffer-gas-cooled and laser-cooled Ca⁺ ions in the linear rf octupole ion trap together with the CFP cavity fringes of the light from the 397-nm laser. The cooling occurs on the red-detuned side of the spectrum. Ion heating and loss from the trap take place on the blue side. Therefore only half of the linewidth is detected and we call this width the half width at half maximum (HWHM). The HWHM of the laser-cooled ions is $\Delta\nu = 108(2)$ MHz, which corresponds to an ion temperature of 12.7(5) K. In this measurement, an ion cloud of about 10^3 ions was present in the octupole trap and the crystal state was not yet realized.

For the present experimental setup, a higher power of the cooling laser is needed to produce the crystal state due to the large trap volume. Alternatively, it is possible to obtain the phase transition LIF spectrum with the present laser power if the number of trapped ions is smaller. To reduce the number of ions, we applied higher static voltages ($V_{z1}, V_{z2} \geq 7$ V) for a few tens of a second. When the static voltages are increased, the trapped ions are heated by the rf fields and a part of the ions escapes from the trap, since the static potential ϕ_s produces potential minima far from the central trap axis in the radial pseudopotential ϕ_{psd} as shown in Figs. 3 and 4. In this way, the number of trapped ions can be reduced if this necessary.

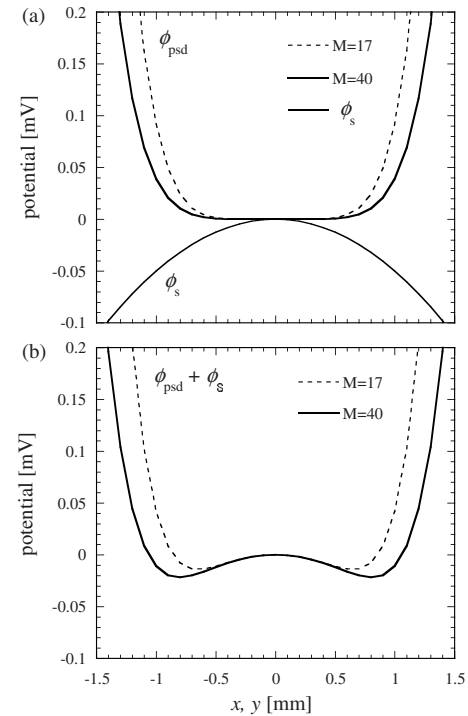


FIG. 3. (a) Static potential ϕ_s and pseudopotential ϕ_{psd} along the x or y axis for the parameters of $f_{\text{rf}} = 10.0$ MHz, $V_{\text{ac}} = 400$ V, $r_0 = 7.5$ mm, $V_{z0} = 0.1$ V, $z_0 = 5$ mm, and $\kappa = 0.025$. The potential curves are calculated for ions with the mass numbers of $M = 17$ and 40. (b) Calculated sum potential of $\phi_{\text{psd}} + \phi_s$ using the result of (a). The heights of the potential barriers in the center are about 0.3 K and 0.5 K for $M = 17$ and 40, respectively. The potential minima are closer to the central trap axis for lighter ions, which may be beneficial for sympathetic cooling.

After reducing the number of trapped ions, we obtain a narrow LIF spectrum with the abrupt dip as depicted in Fig. 5. The dip in the spectrum indicates the phase transition of the trapped Ca⁺ ions from the cloud state to the crystal state [35]. The number of Ca⁺ ions in the crystal state is estimated to be about 200 ions by using the detection efficiency and the estimated LIF rate of 1.5 Mcps/ion at 0.2 mW of the 397-nm cooling laser intensity.

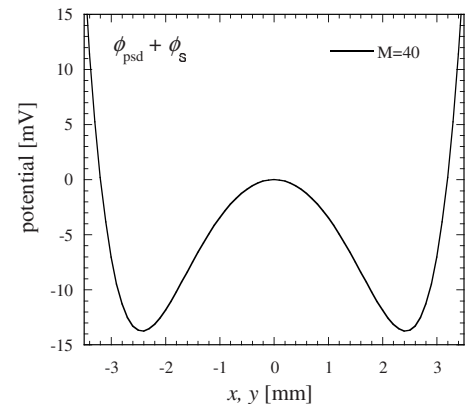


FIG. 4. Calculated sum potential of $\phi_{\text{psd}} + \phi_s$ for the same parameters as in Fig. 3 with the exception of $V_{z0} = 7.0$ V, $f_{\text{rf}} = 9.978$ MHz, and $V_{\text{ac}} = 370$ V.

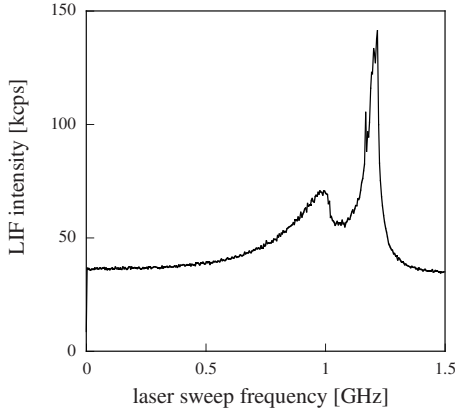


FIG. 5. Fluorescence spectrum of laser-cooled Ca^+ ions. The abrupt dip in the figure shows that the trapped ions form a Coulomb crystal in the linear rf octupole ion trap. The scanning speed of the 397 nm laser is 9.5 MHz/s. The width of the spectrum in the crystal state is $\Delta\nu_{\text{HWHM}}=29(2)$ MHz. Experimental parameters are $f_{\text{rf}}=9.978$ MHz, $V_{\text{ac}}=370$ V, and $V_{z1}=83$ mV, and $V_{z2}=294$ mV.

The radiation pressure force on the trapped Ca^+ ions is not negligible when the laser light is incident into the ion trap in only one direction along the axial direction. For this case, we needed to compensate the radiation pressure effect by applying different axial closing voltages to each set of side electrodes. The influence of the depth of the static potential ϕ_s on the LIF line profile is investigated by taking the laser-cooling spectra at different axial closing voltages as shown in Fig. 6. Here, V_{z2} is fixed at 294 mV while V_{z1} is gradually changed. The position of the dip gradually shifts toward the resonance center as V_{z1} increases. For our particular trap parameters,

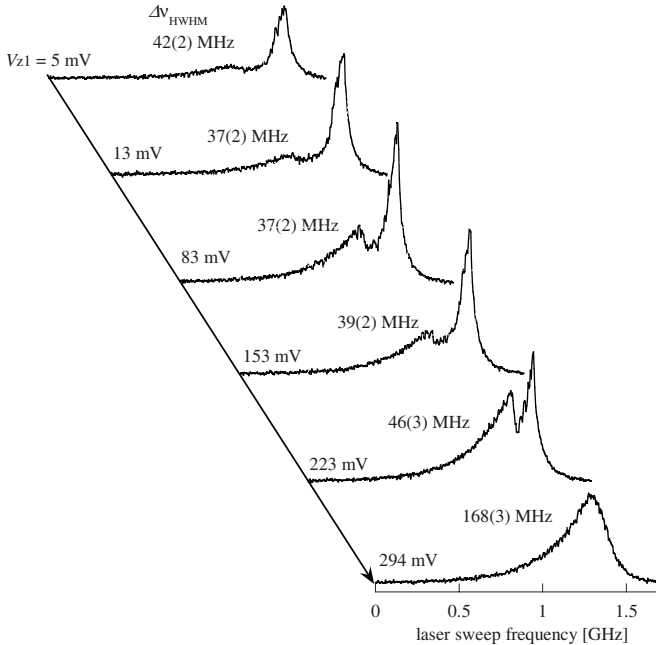


FIG. 6. Fluorescence spectra at different static voltages of V_{z1} . The width (HWHM) of each spectrum in the crystal state (except for $V_{z1}=294$ mV) is indicated. The rf parameters and the voltages of V_{z2} are the same as Fig. 5. The scanning speed of the 397 nm laser is 41 MHz/s. The intensity scale is the same for all spectra.

the optimum static voltage V_{z1} to obtain the narrowest spectrum is found to be about 100 mV. In this case, laser cooling most efficiently dominates rf heating, since the ions are located in a narrow region around the center of the trap where they have good overlap with the laser beam. The spectral width increases when the static voltage V_{z1} is increased above this value, and the trapped Ca^+ ions do not crystallize for $V_{z1} > 290$ mV. The results suggest that excessive closing voltages result in large micromotion amplitudes of the trapped ions. This interpretation is explained in more detail by the results of the MD simulation described in the next section.

III. MOLECULAR DYNAMICS SIMULATION

We carried out a MD simulation to evaluate the general behavior of the dynamics of laser-cooled ions in the linear rf octupole trap and to find the structures of the Coulomb crystals in this geometry. To our knowledge, a MD simulation study for a linear rf multipole ion trap has not been performed yet. In the present experiment, the LIF profiles of the laser-cooled Ca^+ ions are very sensitive to the depth of the static potential ϕ_s ; we expect therefore that the shapes of the Coulomb crystals also change by changing V_{z0} in Eq. (2). This was born out and different structures of the Coulomb crystals are obtained in the MD simulations described in the following.

In the present simulation taking all forces into account, we obtain trajectories and velocities of all the trapped ions by solving Newton's equations of motion. Then we can calculate the average kinetic energy and motional frequency of each trapped ion. The crystal state is reached when laser cooling freezes the trajectories. From the positions of laser-cooled ions in the steady state, the structure of a Coulomb crystal is deduced. Moreover, assuming a two-level system for each laser-cooled ion, the laser-induced fluorescence spectrum from ions can be simulated. Thus, the phase transition LIF spectrum with the abrupt dip is also reproduced.

In more detail the MD simulation is carried out by solving the equations of the ion motion including the trapping forces by the rf octupole field, the axial harmonic field, the Coulomb force (\mathbf{F}_C) between the trapped ions, the radiation pressure force (\mathbf{F}_L), and the averaged recoil force (\mathbf{F}_{sp}) by spontaneous emission according to methods explained in Refs. [36,37]. The Coulomb force for each ion with all the others is given by

$$\mathbf{F}_C = \frac{q^2}{4\pi\epsilon_0} \sum_{i \neq j}^N \frac{\mathbf{r}_i - \mathbf{r}_j}{R_{ij}^3}. \quad (3)$$

The summation index N is the number of ions in the trap. The equations of motion of the i th ion in a linear rf octupole ion trap are then

$$m_i \frac{d^2 x_i}{dt^2} = -\frac{4qx^3}{r_0^4} \left(1 - \frac{3y^2}{x^2}\right) (V_{\text{dc}} - V_{\text{ac}} \cos \Omega t) + \frac{q\kappa V_{z0}}{z_0^2} x + F_{Lx} + F_{Cx} + F_{\text{sp}x}, \quad (4)$$

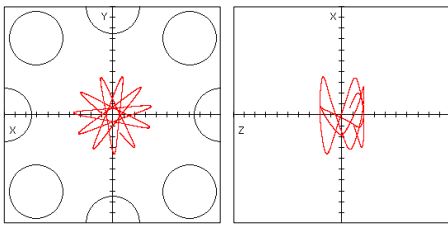


FIG. 7. (Color online) Calculated single Ca⁺ ion trajectory in a linear rf octupole trap. The trapping parameters are set at $f_{\text{rf}} = 10.0$ MHz, $V_{\text{ac}} = 370$ V, $V_{\text{dc}} = 0$ V, $r_0 = 7.5$ mm, $V_{z0} = 1.0$ V, $z_0 = 5$ mm, and $\kappa = 0.025$. The initial conditions of the ion are $(x(0), y(0), z(0)) = (-0.8, 0, 0)$ mm and $(v_x(0), v_y(0), v_z(0)) = (400, -450, 200)$ m/s. The unit on the axes is 1 mm.

$$m_i \frac{d^2 y_i}{dt^2} = -\frac{4qV^3}{r_0^4} \left(1 - \frac{3x^2}{y^2}\right) (V_{\text{dc}} - V_{\text{ac}} \cos \Omega t) + \frac{q\kappa V_{z0}}{z_0^2} y + F_{Ly} + F_{Cy} + F_{\text{sp}y}, \quad (5)$$

$$m_i \frac{d^2 z_i}{dt^2} = -\frac{2q\kappa V_{z0}}{z_0^2} z + F_{Lz} + F_{Cz} + F_{\text{sp}z}, \quad (6)$$

where F_{Lj} and $F_{\text{sp}j}$ ($j = x, y, z$) represent the projection of the radiation pressure and the recoil force onto the j axis. Equations (4)–(6) are numerically solved by the fourth-order Runge-Kutta method [36].

In addition, the effect of elastic collisions by the buffer gas atoms is included, since initially we employ buffer gas cooling before laser cooling. The elastic collision effect is implemented as follows. After each integration step of the Runge-Kutta algorithm, we calculate the mean free path by the equation $\lambda_L = 1/n_g \sigma_L$, where σ_L is the Langevin cross section depending on the collision velocity v . n_g is the number density of the buffer gas. If the flight length of an ion, which is added at each time step, exceeds λ_L , we apply the standard equation for the determination of an ion's velocity after a classical elastic collision [38], where the unit vector of the ion velocity after the collision is given by random numbers.

A short time step of 10 ns was usually used to solve the Newton equations. The value was chosen to be small against the micromotion period and to be able to preserve the initial kinetic energy of a trapped ion for each simulation interval, when the gas collision and the radiation effects are not intentionally included. The number of ions is limited to a few hundred ions due to the available computer power. The total integration time of each cycle is also limited to be less than 1 s and strongly depends on the number of ions.

An example of a simulated trajectory of a single trapped ion is shown in Fig. 7. Here we briefly mention the characteristics of the ion motion. The single ion moves in a straight line except at the turning points. This is due to the pseudo-potential being nearly flat in the radial direction [Fig. 3(a)]. The ion motion frequency mainly depends on the kinetic energy of the ion as long as the adiabaticity condition holds [21].

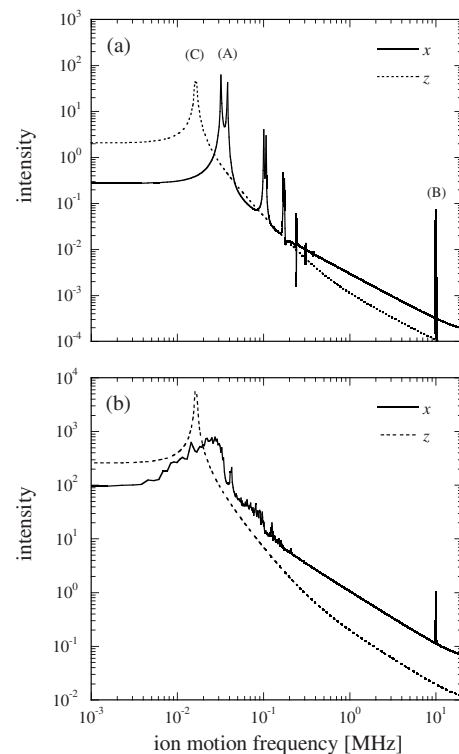


FIG. 8. (a) Spectra of the single-ion motion frequencies of the x and z components. The initial conditions of the ion are $(x(0), y(0), z(0)) = (-0.8, 0, 0)$ mm and $(v_x(0), v_y(0), v_z(0)) = (400, -450, 200)$ m/s. The main peak (A) of the x component is the secular motion frequency depending on the radial component of the velocity. The splitting of the peak is caused by the rosette-like ion motion around the z axis. The contribution of the micromotion frequency f_{rf} (B) and the higher orders of the secular frequencies are also observed. The main peak (C) of the z component is the harmonic vibration frequency, which does not change with the velocity of the ion. (b) Sum spectra of an ion cloud with 120 Ca⁺ ions. For the initial velocities of the ions, a Maxwell distribution with room temperature is assumed. The positions of the ions were set at random. The trapping parameters are the same as in Fig. 7.

As shown in Fig. 8(a), the main peak (A) in the frequency spectrum of the x component shows the secular motion frequency depending on the radial component of the ion velocity. The staying time at the turning points, where the amplitude of the micromotion is large, is short for the single ion and the rf heating effect caused by collisions with residual gases and the other ions is smaller as compared with the case of a quadrupole trap. Since the splitting of the peak is caused by the rosettelike ion motions around the z axis, the splitting is not seen for an ion that passes the origin—i.e., $(x, y) = (0, 0)$. We have confirmed that the peaks will shift to the higher-frequency side for a higher velocity. The splitting of the secular peak will become larger as the angular frequency around the z axis increases.

It should be noted that only for a single ion are the secular frequency peaks sharp. For an ion cloud with a finite energy distribution a broad range of secular oscillation frequencies arises [Fig. 8(b)]. In the MD simulations, we calculate the average kinetic energy of each ion over a period of 500–1000 times the trapping rf period. This averaging time is long

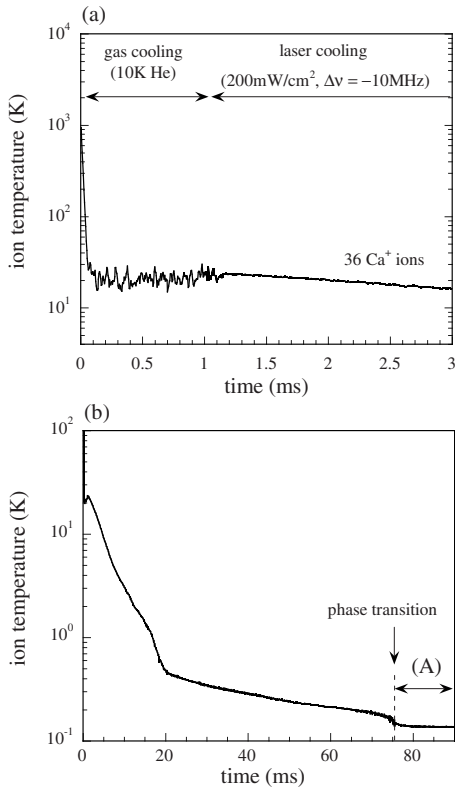


FIG. 9. Time evolution of the temperature of laser-cooled Ca^+ ions ($N=36$) in a linear rf octupole trap. (a) A temporal plot of the temperature of the Ca^+ ions for an integration time of 3 ms. The effect of cold (10 K) gas collisions is introduced for the initial about 1.1 ms. The helium pressure is 10^{-3} Pa. After this time period, the buffer gas pressure is set at 0 Pa, and the radiation pressure force is introduced. (b) A temporal plot of the temperature of the Ca^+ ions for an integration time of up to 90 ms. After 75 ms [indicated by (A)], the ions form a ring-shaped crystal. The trapping parameters are set at $f_{\text{rf}}=10.0$ MHz, $V_{\text{ac}}=400$ V, $V_{\text{dc}}=0$ V, $r_0=7.5$ mm, $V_{z0}=50$ mV, $z_0=5$ mm, and $\kappa=0.025$. The initial average energy of the ions is $E_{\text{ini}}=94$ meV. Counterpropagating laser beams are incident onto the ions under the tilt angles of $\theta=10^\circ$ and $\phi=5^\circ$ relative to the trap axis.

enough to evaluate the average kinetic energy of the ions. Figure 9 shows a simulation result of the time dependence of the average kinetic energy of 36 Ca^+ ions trapped in a linear rf octupole ion trap. The initial average energy of the ions is set to $E_{\text{ini}}=94$ meV and the cold gas collision effect is also applied for the initial 1.1 ms. Thus, the temperature of the ions quickly decreases to about 10 K, which corresponds to the temperature of the buffer gas [Fig. 9(a)].

After the gas-cooling process, the radiation pressure force is introduced in order to include the laser-cooling effect in the MD simulation. At $t=75$ ms, the trapped ions form a Coulomb crystal. This crystal has the ring structure shown in Fig. 10. Although the position of each ion changes depending on the initial conditions, the radius of the ring and the distance between the ions are the same. Such a ring crystal is a unique structure which will be observed in the octupole trap. It has not been observed in experiments using the linear quadrupole Paul trap.

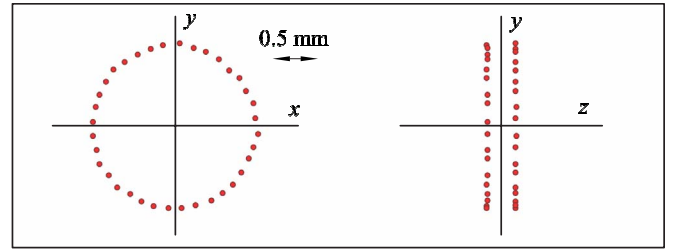


FIG. 10. (Color online). Projection of the spatial structure of the Coulomb crystal with 36 Ca^+ ions under the same condition as those of Fig. 9(a). The radius of each ring crystal and the distance between the rings are ~ 890 μm and ~ 360 μm , respectively.

IV. DISCUSSION

A. Formation of Coulomb crystals

A series of MD simulations has been carried out separately for up to 136 Ca^+ ions to systematically investigate the variation of the structures of Coulomb crystals in the linear rf octupole trap. The results are summarized in Fig. 11. An interesting feature is that as the number of ions increases, the

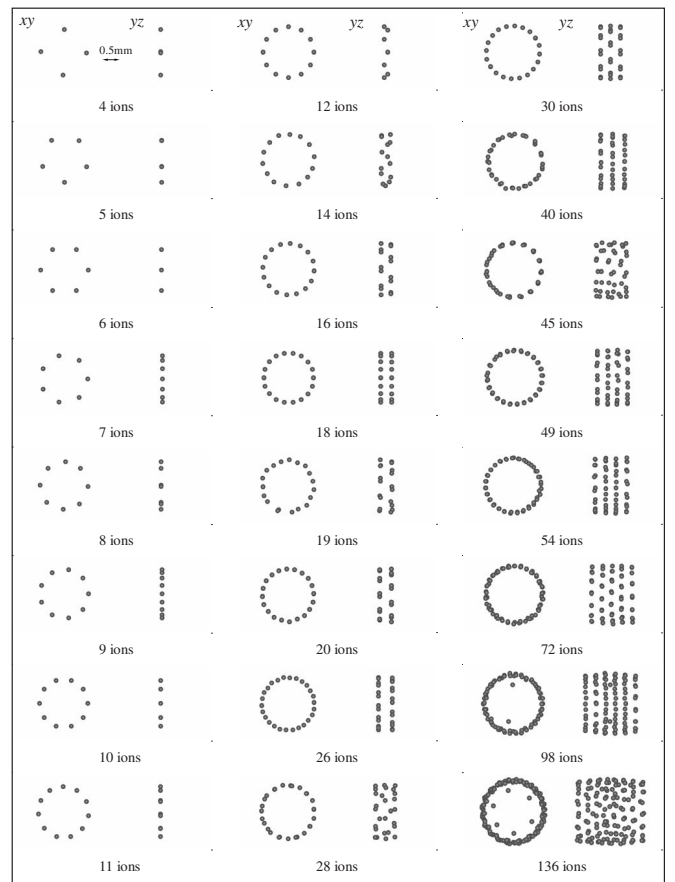


FIG. 11. Projection of spatial structures of Coulomb crystals consisting of Ca^+ ions with $N=4$ to 136. In all figures where the number of ions is different, the scale is made the same. In reality the radius of the ring depends on the number of ions. This dependence is illustrated in Fig. 12(a). The laser parameters and the trapping parameters are the same as in Fig. 9 except for $V_{z0}=25$ mV.

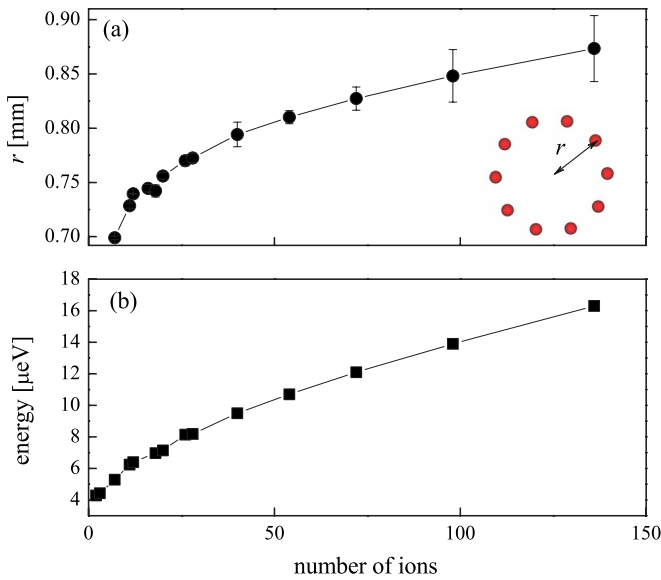


FIG. 12. (Color online) (a) A plot of the average radius of the xy plane of the crystals ($N \geq 7$) depicted in Fig. 11. (b) Average kinetic energy of the Coulomb crystals of Fig. 11. The horizontal axis is the number of ions contained in the Coulomb crystal.

trapped ions form a cylindrical crystal with ring-shaped layers. The maximum number of ions in the first ring crystal is 12 ions in the present simulation. Then, the structure of the Coulomb crystal changes to the two-ring structure ($n=2$) for $N=16$ ions. For the ion crystal containing $N=13-15$ ions, there are different stable structures, which change by variations of the initial conditions of the MD simulations. Similarly, the next transition from $n=2$ to 3 rings occurs for $N=27-29$ ions. This behavior can be understood by the location of the ion motions in the ring-shaped pseudopotential valley [Fig. 3(b)]. The actual position of this valley is determined by the balance between the depth of the sum potential of $\phi_{\text{psd}} + \phi_s$ and the Coulomb potentials between the trapped ions.

Figure 12(b) gives a plot of the average kinetic energy as a function of the number of ions in the crystals. The trend of the average energy is to monotonously increase with N , and no obvious changes are observed near the transition state to additional layers of the rings. This can be understood by the large radii of the ring-shaped crystals, where there is a gradual transition from a ring to a zigzag ring, to the second ring layer crystal, etc., due to the Coulomb repulsion between the ions [Fig. 12(a)]. We find that the number of the rings strongly depends on the axial closing voltage V_{z0} as well as on the number of ions. In order to visualize this effect, MD simulations were performed at different values of V_{z0} for $N=36$ Ca⁺ ions (Fig. 13). The radius of each ring becomes smaller as the static voltage V_{z0} decreases, while the distance between the ring-shaped crystals becomes larger. Since a larger radius of a ring-shaped crystal corresponds to a larger micromotion amplitude of each ion, the average kinetic energy of the ions becomes larger as V_{z0} increases. In actuality, the average energies of the ions depicted in Figs. 13(a)–13(d) are 4.9, 9.1, 44.3, and 137 μeV , respectively (Fig. 14).

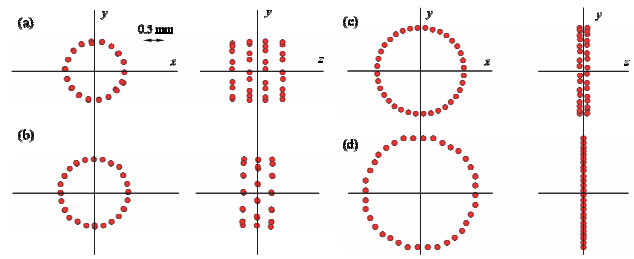


FIG. 13. (Color online) Projection of the spatial structures of the Coulomb crystals of $N=36$ ions at different axial closing voltage V_{z0} of (a) 11.1 mV, (b) 25.0 mV, (c) 110 mV, and (d) 250 mV. The other parameters are same as in Fig. 11.

The effect of V_{z0} is also observed in simulated LIF spectra with the abrupt dips [39]. Figure 15 shows the simulated LIF spectra of six laser-cooled Ca⁺ ions in a linear rf octupole trap. The initial average energy of the ions is set to 50 meV. In the case of $V_{z0}=120$ mV, the abrupt change of intensity is confirmed at about -138 MHz from the center of the resonance. The sharper intensity change than in the experimental spectra is considered to be due to the smaller number of ions. The dip point gradually shifts toward the resonance center as V_{z0} increases. For $V_{z0}=149$ mV and higher, the phase transition does not occur. Considering the simulation results of Fig. 14, the shift of the dip is caused by a slight increase of the rf heating due to an increase of the static voltage V_{z0} which increases the radius of the ion crystal. In such a case, it takes a longer time and a higher cooling rate to cool the ions to below the crystallization temperature. Therefore, the dip point moves forward towards the center of the resonance.

If we change the rf amplitude V_{ac} in the MD simulation, a similar effect as in Fig. 13 can be observed. Figure 16 shows the projection of the ring crystals including ten Ca⁺ ions at

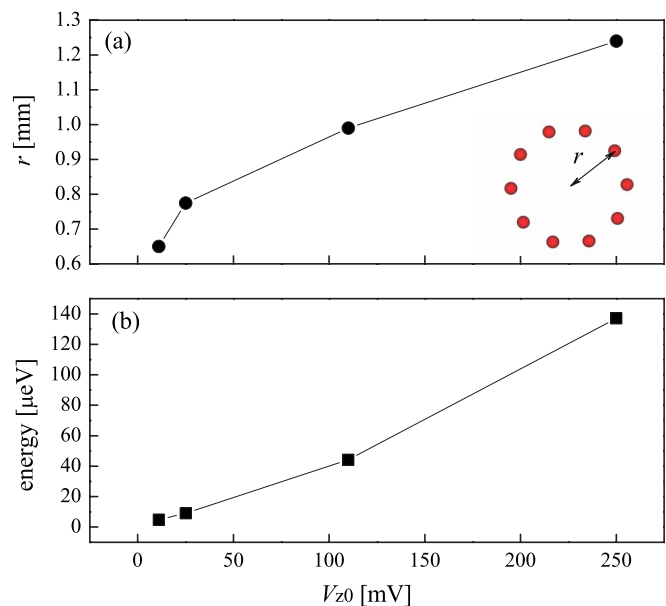


FIG. 14. (Color online) (a) A plot of the average radius of the ring-shaped crystals with Ca⁺ ions ($N=36$) for Fig. 13 as a function of V_{z0} . (b) A plot of the average kinetic energy of the ions for Fig. 13 as a function of V_{z0} .

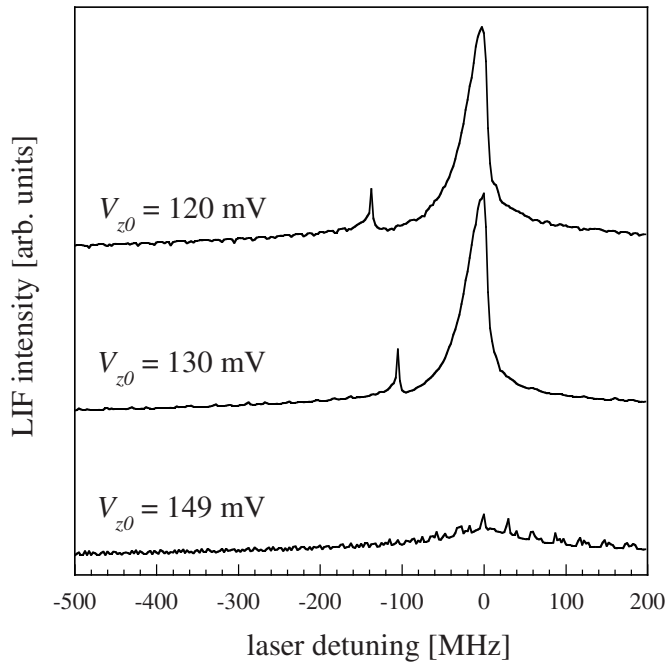


FIG. 15. Simulated LIF spectra of the laser-cooled Ca^+ ions ($N=6$) at different axial closing voltages. The laser frequency is scanned from -800 MHz to 200 MHz at a rate of 25 MHz/ms. The initial average energy of the ions is 50 meV. The laser parameters and the trapping parameters are same as in Fig. 9 except for V_{z0} . The intensity scale is the same for all spectra.

different rf amplitudes. The radius of the ring-shaped crystal decreases as V_{ac} increases. Accordingly, the average kinetic energy of the ions also decreases monotonously, as shown in Fig. 17.

To show the availability of the inner volume of the cylindrical Coulomb crystals, we have performed MD simulations for up to 250 ions. The result is shown in Fig. 18. As the number of ions increases, a new smaller radius ring emerges in the inner part. This is the same situation as in the case of the linear Paul trap, where the small number of ions initially align themselves along the central trap axis like a string. In the case of the linear rf octupole trap, the outer cylindrical part of the Coulomb crystal is initially filled but in the same way the inner portions also are filled up. The number of inner

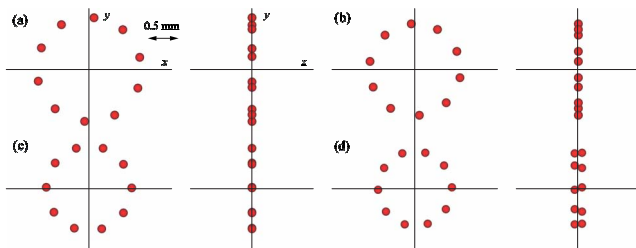


FIG. 16. (Color online) Projection of ring-shaped crystals containing ten Ca^+ ions at different V_{ac} of (a) 300 V, (b) 400 V, (c) 500 V, and (d) 600 V. The static voltage is set at $V_{z0}=25$ mV. The other parameters are the same as in Fig. 11. In the case of $V_{ac}=600$ V, there are different zigzag-ring structures, which depend on the initial condition of the MD simulation.

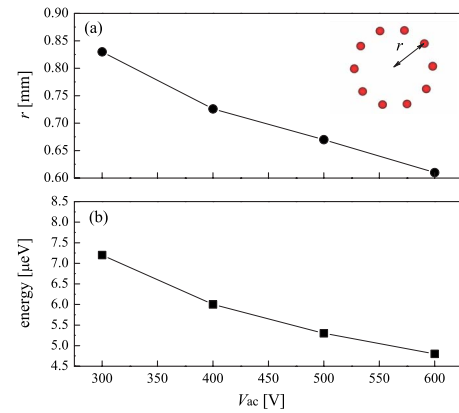


FIG. 17. (Color online) (a) A plot of the average radius of the ring-shaped crystal including ten Ca^+ ions for Fig. 16 as a function of V_{ac} . (b) A plot of the average kinetic energy of the ions for Fig. 16 as a function of V_{ac} . As the amplitude of V_{ac} is further increased, the ring structure becomes obscure; i.e., a zigzaglike structure appears. The mean kinetic energy of the ions gradually decreases to the minimum value of about 1 μeV for the present particular conditions.

rings can be controlled to some degree by changing V_{z0} and the rf amplitude. In the present simulation, we use the static potential of Eq. (2), which is the lowest-order function that satisfies Laplace's equation. Other polynomial closing geometries (set of rings etc.) are under investigation.

The inner part of the cylindrical Coulomb crystals is also available for sympathetic cooling of light molecular ions. As referred to in the Introduction, we obtained the simulation result that the sympathetically cooled light molecular ions by laser-cooled relatively heavy ions are expected to be distributed in the inner part of the outer-ring crystal. This property can be qualitatively understood by the pseudopotential curves shown in Fig. 3(b), where the potential minimum is closer to the central axis for the lighter ion. The inner volume

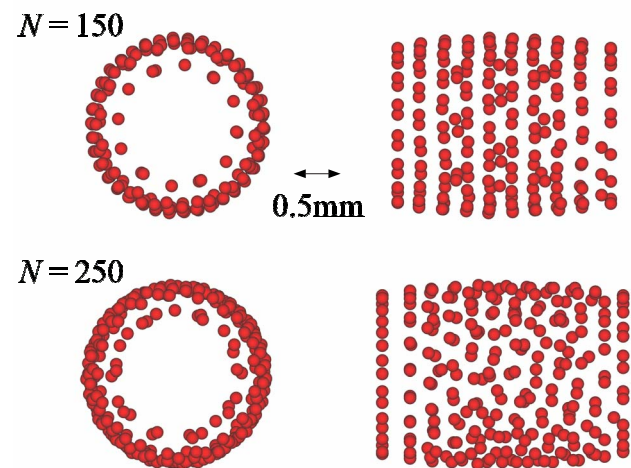


FIG. 18. (Color online) Projection of the cylindrical Coulomb crystals containing $N=150, 250$ Ca^+ ions. The rf amplitude and the static voltage are set at $V_{ac}=400$ V and $V_{z0}=25$ mV, respectively. The other parameters are the same as in Fig. 11.

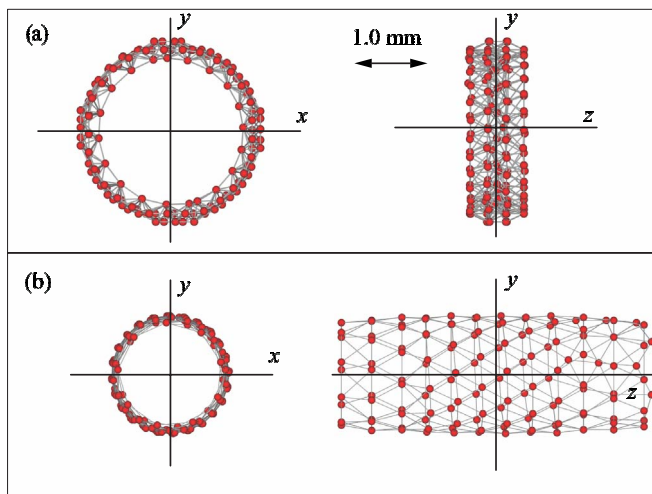


FIG. 19. (Color online) Spatial structure of a large-size Coulomb crystal consisting of $N=136$ Ca^+ ions simulated for (a) $V_{z0}=100$ mV and (b) $V_{z0}=6.3$ mV. The other parameters are the same as in Fig. 11. The connecting lines between ions are added for a clear display of the helical structure.

of the cylindrical Coulomb crystal is available for filling up a larger number of ions and also for sympathetically cooled (or crystallized) light molecular ions.

B. Large-size Coulomb crystal

As mentioned above, the Coulomb crystal in a linear rf octupole trap is very sensitive to the depth of the static potential ϕ_s , and the size of the crystal can be controlled by changing the axial closing voltage V_{z0} . We also demonstrated this process in the MD simulation for a large-size ion crystal. Figure 19 shows the spatial structure of a large ion crystal with 136 Ca^+ ions at two different closing voltages. In the case of Fig. 19(a), a hexagonal structure is observed in the yz projection. If the closing voltage decreases as in the case of Fig. 19(b), the crystal is enlarged in the z axis. Then the spiral structure accompanied by the hexagonal structure emerges in a center part of the surface of the ring-shaped crystals. Since it is possible to manipulate the size and the

structure of a large-size crystal by changing only the static voltage V_{z0} , the Coulomb crystals in a linear rf octupole trap are also an interesting tool for the study of non-neutral plasma physics.

V. SUMMARY

Laser cooling of Ca^+ ions stored in a linear rf octupole trap was performed. The phase transition of the laser-cooled Ca^+ ions is observed by an abrupt dip in the LIF spectrum. We have also systematically observed laser-cooling spectra at different axial closing voltages. By combining the results of the laser-cooling experiment and the MD simulations, it is found that the degree of rf heating of an ion in a linear rf octupole trap is strongly dependent on the axial closing voltages as well as the rf amplitude, both of which determine at which laser detuning the ion crystal state is reached. MD simulations have been performed for up to 250 ions to deduce the structures of Coulomb crystals. We have shown that for a small number of ions a ring-shaped crystal is produced. A cylindrical layer of the rings is formed as the number of ions increases. It is found that we can control the size and the structure of a Coulomb crystal by changing the axial closing voltages and the rf amplitude. In the future, further numerical simulations should be extended to much larger numbers of trapped ions ($N \geq 10^3$) to explore the characteristics of a one-component plasma in linear rf octupole and multipole traps.

The present simulation results can be scaled to an octupole trap with different size electrodes. In experiments where a small size of the ring crystal needs to be produced, one should select a smaller r_0 of the octupole trap. In such a case the solid angle for optical detection becomes smaller. We would like to point out that the linear rf octupole trap and in general multipole traps are promising tools for studying large-ion-number ring-shaped Coulomb crystals.

ACKNOWLEDGMENTS

This work was financially supported in part by Grants-in-Aid for Young Scientists (B) from the Ministry of Education, Culture, Sports, Science and Technology (MEXT), by the Matsuo Foundation, and by the Robert A. Welch Foundation under Grant No. A1546.

-
- [1] J. I. Cirac and P. Zoller, *Phys. Rev. Lett.* **74**, 4091 (1995).
 - [2] C. Monroe, D. M. Meekhof, B. E. King, W. M. Itano, and D. J. Wineland, *Phys. Rev. Lett.* **75**, 4714 (1995).
 - [3] F. Schmidt-Kaler, H. Häffner, M. Riebe, S. Gulde, G. P. T. Lancaster, T. Deuschle, C. Becher, C. F. Roos, J. Eschner, and R. Blatt, *Nature (London)* **422**, 408 (2003).
 - [4] W. M. Itano, J. J. Bollinger, J. N. Tan, B. Jelenković, X.-P. Huang, and D. J. Wineland, *Science* **279**, 686 (1998).
 - [5] A. Mortensen, E. Nielsen, T. Matthey, and M. Drewsen, *Phys. Rev. Lett.* **96**, 103001 (2006).
 - [6] D. H. E. Dubin and T. M. O'Neil, *Rev. Mod. Phys.* **71**, 87 (1999).
 - [7] P. Blythe, B. Roth, U. Fröhlich, H. Wenz, and S. Schiller, *Phys. Rev. Lett.* **95**, 183002 (2005).
 - [8] K. Mølhave and M. Drewsen, *Phys. Rev. A* **62**, 011401(R) (2000).
 - [9] V. L. Ryjkov, X. Z. Zhao, and Hans A. Schuessler, *Phys. Rev. A* **74**, 023401 (2006).
 - [10] J. D. Prestage, R. L. Tjoelker, and L. Maleki, *Phys. Rev. Lett.* **74**, 3511 (1995).
 - [11] H. Müller, S. Herrmann, A. Saenz, A. Peters, and C. Lämmerzahl, *Phys. Rev. D* **70**, 076004 (2004).
 - [12] U. Fröhlich, B. Roth, P. Antonini, C. Lämmerzahl, A. Wicht, and S. Schiller, *Lect. Notes Phys.* **648**, 297 (2004).

- [13] R. Blümel, C. Kappler, W. Quint, and H. Walther, *Phys. Rev. A* **40**, 808 (1989).
- [14] J. D. Prestage, A. Williams, L. Maleki, M. J. Djomehri, and E. Harabetian, *Phys. Rev. Lett.* **66**, 2964 (1991).
- [15] T. B. Mitchell, J. J. Bollinger, D. H. E. Dubin, X. P. Huang, W. M. Itano, and R. H. Baughman, *Science* **282**, 1290 (1998).
- [16] D. H. E. Dubin and T. M. O'Neil, *Rev. Mod. Phys.* **71**, 87 (1999).
- [17] M. Block, A. Drakoudis, H. Leuthner, P. Seibert, and G. Werth, *J. Phys. B* **33**, 1290 (2000).
- [18] T. Schätz, U. Schramm, and D. Habs, *Nature (London)* **412**, 717 (2001).
- [19] M. Drewsen, I. Jensen, J. Lindballe, N. Nissen, R. Martinussen, A. Morttensen, P. Staantum, and D. Voigt, *Int. J. Mass. Spectrom.* **229**, 83 (2003).
- [20] J. P. Schiffer, *Phys. Rev. Lett.* **88**, 205003 (2005).
- [21] D. Gerlich, *Adv. Chem. Phys.* **82**, 1 (1992).
- [22] L. Maleki and J. D. Prestage, *Lect. Notes Phys.* **648**, 331 (2004).
- [23] D. Gerlich and M. Smith, *Phys. Scr.* **73**, C25 (2006).
- [24] E. Herbst, D. J. DeFrees, D. Talbi, F. Pauzat, W. Koch, and D. McLean, *J. Chem. Phys.* **94**, 7842 (1991).
- [25] B. J. McCall, A. J. Huneycutt, R. J. Saykally, T. R. Geballe, N. Djuric, G. H. Dunn, J. Semaniak, O. Novotny, A. Al-Khalili, A. Ehlerding, F. Hellberg, S. Kalhori, A. Neau, R. Thomas, F. Österdahl, and M. Larsson, *Nature (London)* **422**, 500 (2003).
- [26] B. Roth, P. Blythe, H. Wenz, H. Daerr, and S. Schiller, *Phys. Rev. A* **73**, 042712 (2006).
- [27] T. J. Harmon, N. Moazzan-Ahmadi, and R. I. Thompson, *Phys. Rev. A* **67**, 013415 (2003).
- [28] S. Schiller and C. Lämmerzahl, *Phys. Rev. A* **68**, 053406 (2003).
- [29] T. Baba and I. Waki, *Appl. Phys. B: Lasers Opt.* **74**, 375 (2002).
- [30] K. Okada *et al.* *Book of abstracts for the 20th International Conference on Atomic Physics (ICAP 2006)*, p. 495
- [31] K. Okada, M. Wada, T. Nakamura, I. Katayama, L. Boesten, and S. Ohtani, *Jpn. J. Appl. Phys., Part 1* **40**, 4221 (2001).
- [32] K. Okada, M. Wada, T. Nakamura, T. Takayanagi, I. Katayama, and S. Ohtani, *Jpn. J. Appl. Phys., Part 1* **45**, 956 (2006).
- [33] K. Okada, M. Wada, L. Boesten, T. Nakamura, I. Katayama and S. Ohtani, *J. Phys. B* **36**, 33 (2003).
- [34] NIST atomic spectra database version 3.1.0, <http://physics.nist.gov/PhysRefData/ASD/index.html>
- [35] F. Diedrich, E. Peik, J. M. Chen, W. Quint, and H. Walther, *Phys. Rev. Lett.* **59**, 2931 (1987).
- [36] R. Blümel, J. M. Chen, F. Diedrich, E. Peik, W. Quint, W. Schleich, Y. R. Shen, and H. Walther, *Proceeding of the 11th International Conference on Atomic Physics (ELICAP), Paris, 1988* (World Scientific, Singapore, 1989); H. Walther, *Advances in Atomic, Molecular, and Optical Physics* (Academic Press, New York, 1993), Vol. 31, pp 137–182.
- [37] Vladimir L. Ryjkov, XianZhen Zhao, and Hans A. Schuessler, *Phys. Rev. A* **71**, 033414 (2005).
- [38] L. D. Landau and E. M. Lifshitz, *Mechanics (Course of Theoretical Physics)* (Elsevier, New York, 1969).
- [39] X. Z. Zhao, V. L. Ryjkov, and H. A. Schuessler, *Phys. Rev. A* **73**, 033412 (2006).